PERFORMANCE ENHANCEMENT STUDIES IN A THERMOSYPHON FLAT PLATE SOLAR WATER HEATER WITH CuO NANOFLUID

by

Anin Vincely DASAIEN [*] ***and Natarajan ELUMALAI***

Institute for Energy Studies, Anna University, Chennai, India

Original scientific paper
https://doi.org/10.2298/TSCI151005012D

Experiments were conducted on a thermosyphon type flat plate collector, inclined at 45°, for water heating application. Water and water based nanofluids were used as absorber fluid to gain heat from solar rays incident on the flat plate collector. Nanofluids were prepared by adding CuO nanoparticles of 40-50 nm size to the base fluid at 0.1, 0.2, 0.3, and 0.5 wt% (ζ). The hot absorber fluid was made to circulate in the shell side of a heat exchanger, placed at the top of the flat plate collector, where utility water was circulated inside a helically coiled Cu tube. Temperatures at strategic locations in the flat plate collector, working fluid, utility water inlet and outlet were measured. The nanofluid increases the collector efficiency with increasing ζ. A highest efficiency enhancement of 5.7% was observed for the nanofluid with ζ = 0.2 having a mass flow rate of 0.0033 kg/s. The 3-D, steady-state, conjugate heat transfer CFD analyses were carried out using the ANSYS FLUENT 15.0 software. Theoretically estimated buoyancy induced fluid flow rates were close with the CFD predictions and thus validates the computational methodology.

Key words: *thermosyphon flat plate collector, nanofluids, collector efficiency, CFD analysis*

Introduction

Solar thermal energy conversion technologies extract the solar energy and store it by heating an absorber fluid, leading to direct thermal energy conversion. Flat plate collectors (FPC) are widely used for the solar thermal conversion in domestic applications. Out of the total incident solar energy on the FPC, only a small percentage is effectively used for utility application. The overall efficiency of the FPC system will further go down when a pump is used to circulate the absorber fluid. In a thermosyphon FPC, the absorber fluid flows through the inclined collector tubes and rises up to the hot fluid storage tank by buoyancy driven natural convection. Simultaneously, due to gravity, the fluid from the tank descends to the inlet header of the FPC at the bottom. Buoyancy driven solar thermal FPC systems were studied experimentally by several researchers. Chuawittayawuth and Kumar [1] observed experimentally the temperature and flow distribution in a natural circulation solar water heating systems. The temperature variations across and within the absorber tubes were higher on a clear sunny day, while on cloudy days the temperatures were uniform which reflected that the temperature of water in the riser depends on its buoyancy induced flow rate. Hussein [2] investigated theo-

[*] Corresponding author, email: vincely_zeal@yahoo.com

retically and experimentally, the transient thermal behavior of a two-phase thermosyphon FPC and comparison between the experimental and simulated results showed considerable agreement. Nada *et al*. [3] designed a two-phase closed thermosyphon solar collector with a shell and tube heat exchanger. The influence of the cooling water flow rate, the water inlet temperature and number of tubes on the collector performance was experimentally studied.

The low thermal conductivity of water is the primary limitation in the solar thermal system efficiency. A fluid with enhanced thermophysical properties could enhance the performance of the thermosyphon FPC. Nanofluids, the fluids with enhanced physical properties by addition of nanosized metal or metal oxide particles, are being extensively used by several researchers. The term *nanofluid* was first coined by Choi and Eastman [4]. Wang *et al*. [5] measured thermal conductivity in nanofluids containing Al_2O_3 and CuO nanoparticles. Agglomeration of nanoparticles with aging, pose a greater challenge to the widespread application of nanofluids in engineering. Lee *et al*. [6] suggested ultrasonic vibration of nanofluids and addition of surfactants helps in enhancing the suspension of nanoparticles. Yousefi *et al*. [7] investigated Al_2O_3-water nanofluid and used Triton X-100 as surfactant to increase the stability of the nanofluid. Their nanofluid with $\zeta = 0.2$ showed efficiency 28.3% higher than that of water.

Goudarzi *et al*. [8] investigated experimentally the performance for a cylindrical solar collector with helical pipe receiver. The results showed that for CuO nanofluid of $\zeta = 0.1$ and 0.0083 kg/s flow rate, the collector efficiency increased by 25.6% than with water. Ali Jabari *et al*. [9] studied the effect of CuO-water nanofluid on FPC efficiency and found that there exists an optimum mass flow rate which maximizes the collector efficiency. From these studies, it was decided to use CuO based nanofluid for the present study. However, the previous cited works employed a pump for the forced circulation of the nanofluid. Computational investigations on a thermosyphon based FPC system are limited. Selmi *et al*. [10] employed a CFD package CFDRC to analyze the flat plate collector and found that the validation was satisfactory.

A review of the studies on the application of nanofluids in solar thermal systems was previously summarized. However, nanofluid application in a thermosyphon FPC (without using an external pump) is relatively new and reported research work was found to be minimal. The uniqueness of the present work is the usage of CuO nanofluid as the absorber fluid for the FPC. A closed loop thermosyphon FPC was chosen for the present study, as the fluid temperature will increase continuously which will help in maintain buoyancy in the system. Thus the objective of the present study is to investigate experimentally and computationally, the influence of concentration of CuO based nanofluid on the performance enhancement of a closed loop thermosyphon FPC, without any external pump to drive the absorber fluid.

Experimental methodology

The FPC set-up was placed in the roof top of a building so that the FPC gets the maximum exposure to sunlight without any shadow effects. Fluid circuit and instrumentation connections were made in the set-up and initially water was used as the absorber fluid with utility water to receive heat from FPC. Later experiments were conducted with nanofluids as the absorber fluid to study the performance enhancement. The details of the experimental set-up and instrumentation used are discussed in this section.

Experimental set-up and test procedure

Figure 1 show the schematic sketch of the experimental set-up which consists of a thermosyphon type FPC (2) through which the nanofluid circulates and a Cu tube double pipe heat exchanger – HX (1) through which the utility water circulates. The fluid circuit loop and system components are highlighted. An absorber fluid was initially filled inside the HX (1) and FPC (2) assembly before the start of the experiments. When positioned towards the solar radiation, the absorber fluid at the HX flows into the FPC by gravity in the negative z-direction through a flexible rubber hose. The absorber fluid enters the inlet header (4) made of Cu and gets distributed to the riser tubes (5) made of Cu.

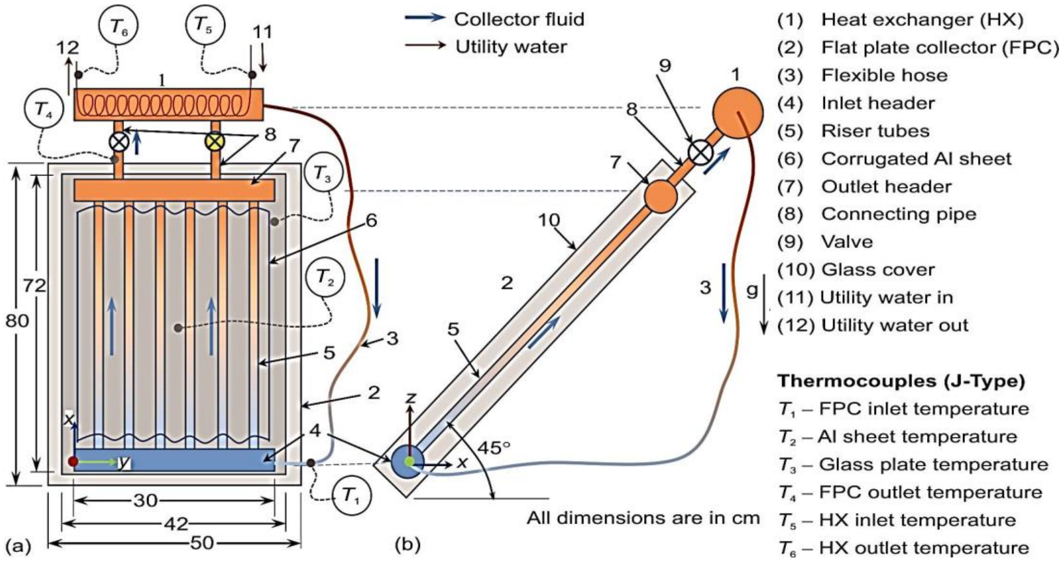

Figure 1. Schematic sketch of the experimental set-up; (a) plan view, (b) side view

The absorber fluid gets heated by the solar insolation received by the corrugated aluminum sheet (6) connected to the riser tubes to enhance the exposed surface area. The sheet was joined to the riser tube by welding at multiple spots and coated with lamp black to enhance absorption. This assembly was placed inside the FPC and covered with a glass (10). The heated absorber fluid moves up inside the riser tubes due to buoyancy. Thus a small quantity of the absorber fluid starts flowing in the system naturally and a circulation is triggered. The absorber fluid from the riser tubes flows into the outlet header (7) and gets collected in the HX through connecting tubes (8). The inlet, outlet headers and the riser tubes were placed above a densely packed glass wool packing in the FPC, to avoid any thermal loss to the bottom side. The connecting tubes were provided with valves (9) to operate the absorber fluid on the shell side and the utility water on the tube side in parallel/counter flow configurations. The right side connecting tube valve was closed in the present experiments to effect counter flow arrangement. Utility water enters the HX from the right side inlet (11) and flow towards the left and exits through the outlet (12). The J-type thermocouples, as shown in fig. 1, were used for measuring the temperatures at strategic locations. The HX is of shell and coil type made of Cu and insulated. The connecting pipelines to the HX are also thermally insulated to reduce the heat loss. The dimensions of the shell used in the HX are 55 mm diameter and 400 mm long. The shell contained a helical coiled Cu tube of 6 mm diameter, 4500 mm length, and 1 mm thick. The thickness of the corrugated aluminum fins attached to the riser tube was 0.5 mm. The flow rate of the absorber fluid was controlled by using valves. The utility water and the absorber fluid flow rates were compared by measuring the fluid over a certain period of time in a measuring jar. A storage tank of 30 liter capacity was used for the utility water circulation, not shown in figure, where its temperature increases continuously.

Preparation of nanofluids

The CuO nanopowders of 40 nm size were added to DI water, which was used as the base fluid in the present study, to prepare nanofluids. CuO nanoparticle was purchased from Sigma Aldrich Chemicals Ltd., USA. Nanofluids of different nanoparticle weight concentration, ζ, were prepared by dispersing CuO nanoparticles. The nanoparticles are initially mixed with the base fluid and placed in a magnetic stirrer for an hour. In order to enhance the nanoparticle dispersion, the nanofluid was then subjected to ultrasonic vibrations by using Equitron™ 2500 ultrasonic sonicator for a period of 3 to 4 hours. Sodium dodecyl benzene sulfonate was used as the non-ionic surfactant and dispersing agent at a ratio of 1:10.

Figures 2(a) and 2(b) shows the SEM images of CuO nanoparticle taken before conducting the experiments, at different zoom levels which indicates that its morphology is spherical and shows tiny agglomerates only. Figures 2(c) and 2(d) shows the high resolution transmission electron microscopy (HR-TEM) image of the CuO nanofluid at 50 nm and 2 nm, respectively. The TEM images show better dispersion of nanoparticles. Prior to the experiments the nanofluid stability was tested by storing the nanofluid samples of different concentrations in glass containers, and monitored for sedimentation up to 10 days. It was observed that the color and uniformity of the corresponding samples remain unaltered, indicating the stability of nanofluids.

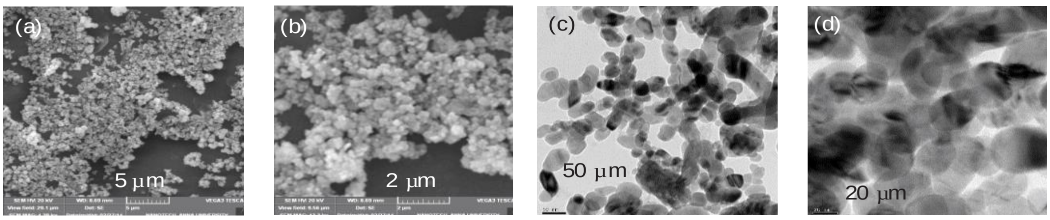

Figure 2. The SEM and HR TEM photographs of CuO nanoparticle suspension with ζ = 0.2

In the present experiments, buoyancy force drives the working fluid, and there is a possibility for the nanoparticles to settle down inside the FPC. The density of the nanofluid was measured prior to and after the experiments to ensure that sedimentation is not occurring in FPC, for all concentrations. The measurements revealed that the change in density was only 1.3, 2.5, 2.8, and 3.7%, respectively, for the nanofluids with ζ = 0.1, 0.2, 0.3, and 0.5. Thus the sedimentation issue did not surface in this set-up. The detailed specifications of the thermosyphon FPC are provided in tab. 1.

Thermophysical properties of nanofluids

The thermophysical properties of the nanofluids were estimated theoretically following the correlations of Vajjha and Das [11]. The specific heat and density is calculated following the equations of Pak and Cho [12], and viscosity from Brinkman [13]. Density was estimated experimentally by measuring the mass of the known volume of the nanofluid. The thermal conductivity was experimentally measured using KD2-pro thermal property meter which works on the basis of transient hot wire method. The measurements were repeated thrice to confirm the repeatability of the measured value. Viscosity was measured experimentally using a parallel plate rheometer (Malvern Bohlin Gemini Rotonetic 2 drive) for the prepared nanofluid. The properties of the CuO nanofluid thus obtained from the correlations and experiments are given in tab. 2. The experimentally measured thermal conductivity values are found to be in agreement with that of the calculated values, thus providing confidence on the measured values.

Table 1. Specifications of the thermosyphon type FPC

Specification	Unit	Dimension
Occupied area, absorption area, A_c	mm^2	800 × 500, 720 × 420
Diameter of upper and lower header, OD	mm	25
Length of the upper and lower header	mm	300
Diameter, length of the riser, OD	mm	12600
Specific heat of water, C_p	J/kgK	4180
Specific heat of nanoparticle, C_{np}	J/kgK	551
Density of nanoparticle, ρ_{np}	kg/m^3	6300

Table 2. Properties of CuO nanofluid at 35 °C

ζ [%]	φ [%]	Density [kgm^{-3}]		Specific heat capacity [Jkg^{-1}K^{-1}]	Thermal conductivity [Wm^{-1}K^{-1}]		Viscosity [Nsm^{-2}] × 10^{-3}	
		Pak and Cho [12]	Expt.	Pak and Cho [12]	Vajha and Das [11]	Expt.	Brinkman [13]	Expt.
0.1	0.015	1079	1035	4123	0.627	0.634	0.74	0.77
0.2	0.032	1169	1108	4065	0.654	0.663	0.78	0.82
0.3	0.047	1249	1153	4008	0.681	0.691	0.81	0.89
0.5	0.079	1418	1260	3892	0.740	0.751	0.88	1.05

Efficiency calculations and uncertainty analysis

The useful energy gain by the collector is calculated in terms of the energy absorbed and lost. The correlations for the instantaneous collector efficiency, the heat removal factor and the collector efficiency factor can be obtained from Duffie and Beckman [14] and hence were not reproduced here.

Uncertainty analysis is needed to prove the accuracy of the experiments and used presently following Abernethy *et al.* [15]. The wind speed was implemented by a PROVA (AVM-07) anemometer type with ±2% accuracy. The error for TM-207 solar power meter was about ±2%. The error for the J-type thermocouple for temperature measurement is ±0.2°C.

The experimental uncertainties of the collector efficiency $U_{\eta i(x)}$ can be calculated:

$$U_{\eta_{\mathrm{i}(x)}} = \eta_{\mathrm{i}} \sqrt{\left(\frac{U_{F_R}}{F_R}\right)^2 + \left(\frac{U_{U_L}}{U_L}\right)^2 + \left(\frac{U_{\Delta T_{\mathrm{ia}}}}{\Delta T_{\mathrm{ia}}}\right)^2 + \left(\frac{U_{G_T}}{G_T}\right)^2} \tag{1}$$

where U_{F_R} can be calculated as the following relation with considering the negligible error in A_c:

$$U_{F_R} = F_R \sqrt{\left(\frac{U_{\dot{m}}}{\dot{m}}\right)^2 + \left(\frac{U_{\Delta T_{\mathrm{ia}}}}{\Delta T_{\mathrm{ia}}}\right)^2 + \left(\frac{U_{\Delta T_{\mathrm{oi}}}}{\Delta T_{\mathrm{oi}}}\right)^2 + \left(\frac{U_{G_T}}{G_T}\right)^2 + \left(\frac{U_{U_L}}{U_L}\right)^2} \tag{2}$$

$$U_{U_L} = U_L \sqrt{\left(\frac{U_{h_{\mathrm{rad}}}}{h_{\mathrm{rad}}}\right)^2 + \left(\frac{U_{h_{\mathrm{wind}}}}{h_{\mathrm{wind}}}\right)^2 + \left(\frac{U_{h_{\mathrm{air}}}}{h_{\mathrm{air}}}\right)^2 + \left(\frac{U_{\Delta T_{\mathrm{oi}}}}{\Delta T_{\mathrm{oi}}}\right)^2 + \left(\frac{U_{h_{\mathrm{fluid}}}}{h_{\mathrm{fluid}}}\right)^2} \tag{3}$$

where $U_{h\mathrm{rad}}$, $U_{h\mathrm{wind}}$, $U_{h\mathrm{air}}$, $U_{h\mathrm{fluid}}$, and $U_{\Delta T\mathrm{oi}}$ are, respectively, the uncertainties of h_{rad}, h_{wind}, h_{air}, h_{fluid}, and ΔT_{oi} (temperature rise across the collector).

$U_{\dot{m}}/\dot{m} \leq 0.2\%$, $U_{h\mathrm{rad}}/h_{\mathrm{rad}} \leq 0.89\%$, $U_{h\mathrm{wind}}/h_{\mathrm{wind}} \leq 0.57\%$, $U_{h\mathrm{air}}/h_{\mathrm{air}} \leq 0.125\%$, $U_{\Delta T\mathrm{oi}}/\Delta T_{\mathrm{oi}} \leq 0.316\%$, $U_{h\mathrm{fluid}}/h_{\mathrm{fluid}} \leq 0.33\%$, $U_{UL}/U_L \leq 1.16\%$, $U_{GT}/G_T \leq 2\%$, $U_{\Delta T\mathrm{ia}} \leq \Delta T_{\mathrm{ia}} \leq 0.3\%$, $U_{FR}/F_R \leq 2.36\%$, and the maximum uncertainty in the collector efficiency was estimated as 3.32%.

Computational methodology

Numerical investigations was based on 3-D steady-state conjugate heat transfer analysis to infer flow and heat transfer characteristics of the absorber fluid using the finite volume based CFD code ANSYS FLUENT 15.0. The objective of the present CFD analysis was to validate the computational methodology adopted presently and to understand the system characteristics in detail, which would otherwise be difficult. For any thermal CFD analysis, it needs accurate thermal boundary condition for an accurate prediction. The temperature gain of the absorber fluid depends mainly on the incident heat flux.

Computational domain

The computational model built with reference to the physical model tested in the experiments is shown in fig. 3 was modeled in a conjugate fashion. The right side tube connection to the HX from the outlet header was not modeled as the flow through that pipe was blocked in the experiments. Grid independency tests are carried out for the FPC with the surface averaged fluid outlet temperature as the assessment criteria. Figure 4 shows the variation of numerical fluid outlet temperature with different mesh densities. The temperature value increases by 5.7% when the mesh was increased from 4.3 to 6.8 million cells. The corresponding change from 6.8 to 9.7 million cells is 1.36% only. This indicates that the mesh density beyond 6.8 million cells is insignificant and hence it was used for the present study. Pre-processing tool Gambit 2.4 was used to produce finer near wall meshing and the solution independent mesh of the FPC domain is shown in fig. 5. Hybrid meshing with a combination of hexahedral and tetrahedral mesh elements was used throughout the computational domain. Figure 5(a) shows the meshed outlet header region and the corrugated sheet whereas and fig. 5(b) shows the meshed HX.

Numerical method

The fundamental governing equations for flow and heat transfer are the continuity, momentum (Navier-Stokes) and energy equations. Based on the mass flow rate and geometry, the Reynolds numbers are found to fall well below the critical value and hence the flow can be treated as laminar. More details of the governing equations can be found in [16] and hence not reproduced here for conciseness. Presently the flow induced in the FPC is due to thermosyphon effect, predominantly controlled by buoyancy effect and hence laminar viscous model was chosen. Buoyancy is included in the solver by enabling Boussinesq approximation

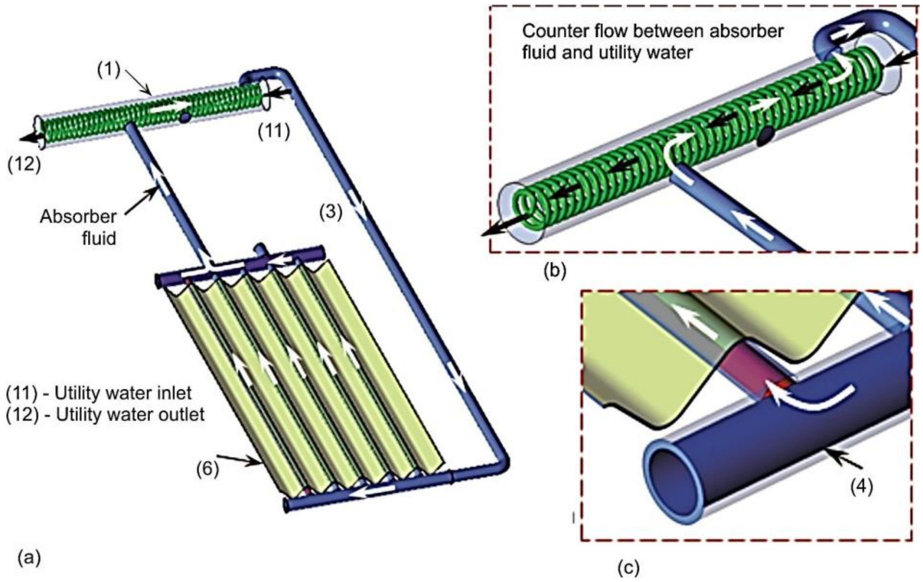

Figure 3. Computational domain of the thermosyphon FPC; (a) FPC, (b) heat exchanger, and (c) inlet header

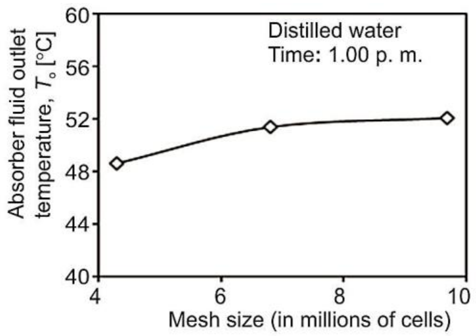

Figure 4. Fluid temperature variation with mesh density

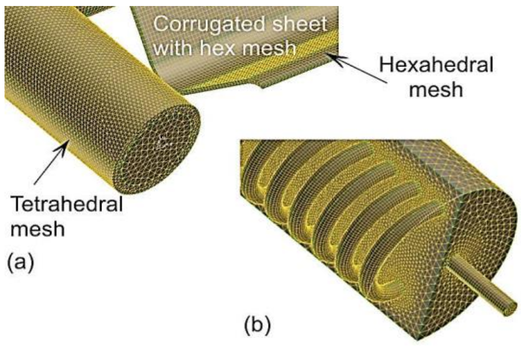

Figure 5. Meshed computational domain; (a) outlet header region, (b) heat exchanger

in the material properties with a suitable thermal expansion coefficient. The SIMPLE scheme was used for the pressure velocity coupling and second order up-winding was chosen for discretization of the governing equations. The CFD computations were carried out for the heat flux measured at 1.00 p. m. hours from the experiments. The FPC assembly was housed inside a glass cover with mineral wool insulation in the bottom and hence treated adiabatic in the computations. The influence of radiation heat transfer is negligible, considering the operating temperature range, and hence not included. The material properties of the nanofluid were fed as inputs to the CFD solver. The convergence criterion was set as 10-5 for all the governing parameters. The boundary conditions used are:

– constant heat flux, $q'' = 1020$ W/m^2 : absorber sheet top surface
– constant heat flux, $q'' = 0$ W/m^2 : riser tube bottom surfaces, connecting tubes to HX

– specified mass flow rate, $\dot{m}$ = c kg/s : heat exchanger inlet
– specified static pressure, Ps = c Pa. : heat exchanger outlet

Results and discussion

Experiments were conducted for several days between 10 a. m. and 4 p. m. The maximum variations in ambient and inlet temperature in each test period are 0.7 °C and 0.5 °C, respectively, whereas the maximum variation in the global radiation was 28 W/m^2.

Experiments with base fluid

A typical set of recorded experimental data in one of the test days, for the heat exchanger fluid (utility water) flowing at 0.0033 kg/s showed a maximum temperature of 81 °C on the absorber plate. A highest temperature difference of 6 °C was observed between the fluid inlet and fluid outlet at 1:30 p. m. with a corresponding insolation of 1108 W/m^2. The maximum fluid outlet temperature was found to be 51 °C for this case. As reported by Koffi *et al*. [17], on a sunny day, the maximum value of the collector outlet temperature as reported by several authors ranged between 70-76 °C. In order to compare collectors of different absorber area, it will be appropriate to compare the thermal efficiency of the system under study, which will be discussed subsequently.

Experiments with nanofluids

A highest temperature difference of 8 °C with a maximum absorber fluid outlet temperature of 53 °C was found for the nanofluids. Figure 6 compares the efficiency of the FPC using water and CuO nanofluid with ζ = 0.2, with a utility fluid flow rate of 0.0033 kg/s. Values of $F_R U_L$ and $F_R(\tau\alpha)$ are calculated and represented in tab. 3. The $F_R(\tau\alpha)$ is the intersection of the line with the vertical axis and nominated as absorbed energy parameter. The value of $F_R U_L$ that is the slope of the line is nominated as the removed energy parameter. As shown in tab. 3, the F_R $(\tau\alpha)$ and $F_R U_L$ values for nanofluid were increased 5.7% and 29.7%, respectively, in comparison with water. The increase in the maximum thermal efficiency, F_R $(\tau\alpha)$ can compensate the increase in removed energy parameter, $F_R U_L$. Therefore, it can be concluded that the efficiency of the solar collector was increased when using CuO nanofluids as compared to that using water.

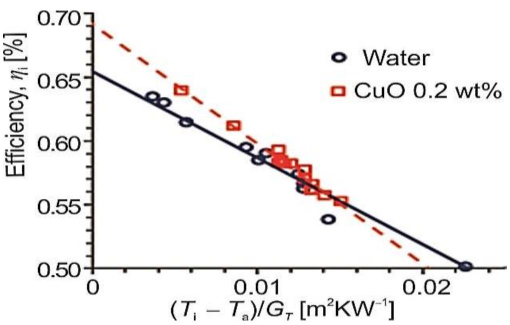

Figure 6. The FPC efficiency with water and CuO nanofluid

Table 3. Values of $F_R U_L$, F_R $(\tau\alpha)$ and R^2 for water and CuO nanofluid (ζ= 0.2)

Base fluid type	$F_R U_L$	F_R $(\tau\alpha)$	R^2
Water	6.7733	0.6546	0.970
CuO nanofluid ζ= 0.1	9.1096	0.6753	0.9945
ζ= 0.2	9.3913	0.6916	0.974
ζ= 0.3	7.9034	0.6686	0.992
ζ= 0.5	10.292	0.6806	0.994

Effect of nanofluid concentration

The efficiency of FPC *vs*. the reduced temperature parameter for different concentrations of CuO nanofluid at different ζ = 0.1, 0.2, 0.3, and 0.5 is shown in fig. 7(a). It was observed that the efficiency of FPC for ζ = 0.2 was higher than that of all other concentrations. Ding *et al*. [18] provided that the local heat transfer coefficient, h, can be approximately given as k/δ_t where k and δ_t are thermal conductivity and the thickness of thermal boundary-layer, respectively. Based on this, it may be concluded that the increasing k_{nf} compare to k_{bf} is smaller than the increasing of thermal boundary-layer. Therefore, a decrease in heat transfer can be justified. As can be seen from tab. 3, increasing ζ from 0.1 to 0.2 $F_R(\tau\alpha)$ and F_RU_L was increased about 2.4% and 3.1%. However, with increase of ζ from 0.2 to 0.5 $F_R(\tau\alpha)$ decreased by 1.6% and F_RU_L increased by 9.6% which means that the collector efficiency was decreased.

Figure 7(b) shows the variation of the efficiency *vs*. reduced temperature parameter, $(T_\mathrm{i} - T_\mathrm{a})/G_T$ for mass flow rates of 0.0016 and 0.0033 kg/s for nanofluid with $\zeta = 0.2$. The $F_R(\tau\alpha)$ and F_RU_L values of the solar collector for various mass flow rates of CuO nanofluid are represented in tab. 4. It can be concluded that for small values of reduced temperature differences parameter $(T_\mathrm{i} - T_\mathrm{a})/G_T$, the efficiency is increased by increasing the mass flow rate. Beyond these small values, the efficiency gets a reverse trend. Therefore, due to increase of mass flow rate, the bulk temperature of CuO nanofluid is decreased. Thus its thermal conductivity enhancement is reduced.

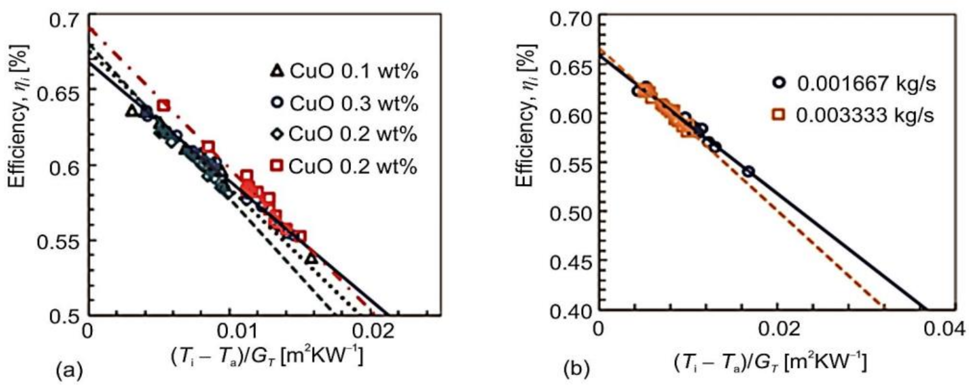

Figure 7. Effect of property variation of nanofluid on the FPC efficiency; (a) mass concentration, (b) mass flow rate

Effect of mass flow rate

Figure 8 shows the variation of the solar insolation on the different days of the experiments with base fluid and nanofluid. The corresponding changes in the mass flow rate of the absorber fluid in FPC are also shown in the same figure. It was observed that the mass flow rate of the working fluid is mainly dependent on the solar insolation, as the flow induced is driven by buoyancy. Comparing two nanofluid concentrations, it can be observed that the increased addition of the nanoparticle has a lesser influence on the induced absorber fluid flow rate. Figure 9 shows the strong dependence of the system efficiency on the absorber fluid flow rate, which increases with solar radiation.

Table 4. Values of F_RU_L, $F_R(\tau\alpha)$ and R^2 for CuO nanofluid with different mass flow rate

Flow rate [kgs^{-1}]	F_RU_L	$F_R(\tau\alpha)$	R^2
0.0016	7.031	0.6589	0.977
0.0033	10.292	0.6806	0.994

It reaches its maximum value of 64.3% for an optimal mass flow rate of 0.00695 kg/s. Comparison of the overall efficiency values estimated presently with that of Koffi *et al*. [17], showed that the present experiments with nanofluids showed higher efficiency at all flow rates. The thermal efficiency from the computations was also added and the computational results showed good agreement with the experimental values. Thus the present computational approach was vindicated.

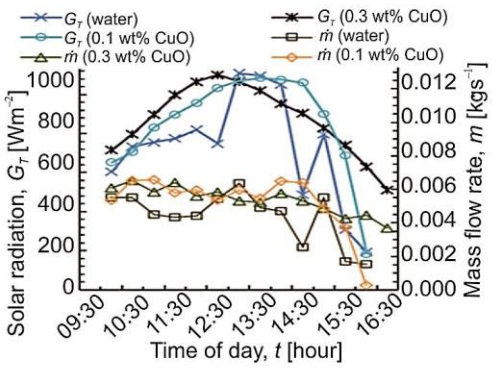

Figure 8. Solar radiation and absorber fluid flow rate variation with time

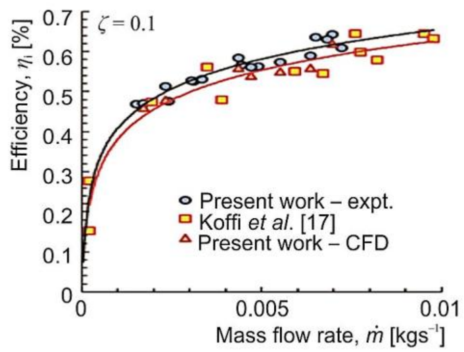

Figure 9. Collector efficiency variation with absorber fluid flow rate

Results from CFD with nanofluid

The contours of temperature on the wall surfaces of the computational domain with a nanofluid of $\zeta = 0.1$ is shown in fig. 10(a). Higher temperatures were observed on the free ends of the corrugated sheet whereas the regions of the sheet touching the riser tubes were relatively cold. It is difficult to measure the coolant fluid flow rate experimentially and hence computational approach was resorted. Good agreement of the absorber fluid flow rate between the present computations and theoretically estimated values was found. Figure 10(b) shows the temperature contours on the mid plane passing through the domain. As the absorber fluid rises up its temperature was found to increase. Peak temperature was found in a region close to the top header and moves towards the HX where it transfers heat to the utility water.

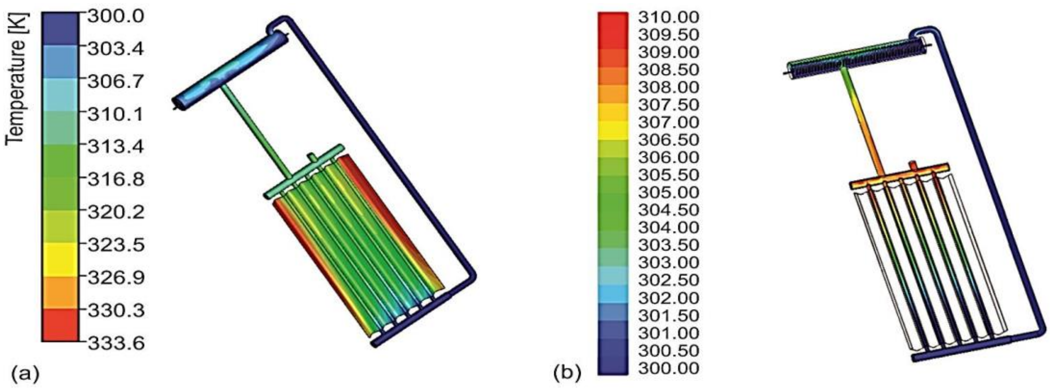

Figure 10. Temperature distribution on the thermosyphon FPC ($\zeta = 0.1$); (a) wall surfaces of the domain, (b) mid plane passing through domain
(*for color image see journal web site*)

Conclusion

Experiments were conducted to study the effects of using CuO nanofluid as the absorbing medium on the efficiency of the flat-plate solar collector, with input information about the effects of mass flow rate of nanofluid with different mass concentration of nanoparticles. An enhancement in efficiency of 5.7% for a mass flow rate of 0.0033 kg/s by using CuO nanofluid is observed from the experimental results. The optimum mass flow rate depends on the thermal characteristics of working fluid. For small values of reduced temperature differences parameter, the efficiency is increased by increasing the mass flow rate and the efficiency decreases if this parameter increases beyond certain value and gets a reverse trend. A maximum efficiency of 64% is achieved in the present collector for CuO nanofluid with $\zeta = 0.2$. The present analysis experimentally and computationally confirms the use of CuO nanofluid for enhanced performance of thermosyphon flat plate collector.

Nomenclature

A_C – surface area of solar collector, [m^2]
C_p – heat capacity, [Jkg^{-1}K^{-1}]
F' – collector efficiency factor. [–]
F_R – heat removal factor, [–]
G_T – global solar radiation, [Wm^{-2}]
$\dot{m}$ – mass flow rate of fluid flow, [kgs^{-1}]
Q_u – rate of useful energy gained, [W]
t – time, [s]
T – temperature, [K]
U_L – overall loss coefficient, [Wm^{-2}K^{-1}]
K_B – Boltzmann constant [–]
k – thermal conductivity, [Wm^{-1}K^{-1}]

Greek symbols

$\tau\alpha$ – product of absorbance and transmittance
η_i – instantaneous collector efficiency
ζ – volume fraction of nanoparticles
ρ – density [kgm^{-3}]

Subscripts

a – ambient
bf – base fluid
i – inlet
np – nanoparticle
nf – nanofluid
o – outlet
tp – tube outlet side of the absorber
eff – effective

References

[1] Chuawittayawuth, K., Kumar, S., Experimental Investigation of Temperature and Flow Distribution in a Thermosyphon Solar Water Heating System, *Renew Energy, 26* (2002), 3, pp. 431-448
[2] Hussein, H. M. S., Optimization of a Natural Circulation Two Phase Closed Thermosyphon Flat Plate Solar Water Heater, *Energy Conversion and Management, 44* (2003), 14, pp. 2341-2352
[3] Nada, S. A., *et al*., Performance of a Two-Phase Closed Thermosyphon Solar Collector with a Shell and Tube Heat Exchanger, *Applied Thermal Engineering, 24* (2004), 13, pp. 1959-1968
[4] Choi, S. U. S., Eastman, J. A., Enhancing Thermal Conductivity of Fluids with Nanoparticles, *Proceedings*, ASME International Mechanical Engineering Congress and Exhibition, San Francisco, Cal., USA, 1995
[5] Wang, X., *et al*., Thermal Conductivity of Nanoparticle – Fluid Mixture, *J. Thermophysics and Heat Transfer, 13* (1999), 4, pp. 474-480
[6] Lee, S., *et al*., Measuring Thermal Conductivity of Fluids Containing Oxide Nanoparticles, Transaction of ASME, *J. Heat Transfer, 121* (1999), 2, pp. 280-289
[7] Yousefi, T., *et al*., An Experimental Investigation the Effect of Al_2O_3-H_2O Nanofluid on the Efficiency of Flat-Plate Solar Collectors, *Renew Energy, 39* (2012), 1, pp. 293-298
[8] Goudarzi, K., *et al*., An Experimental Investigation on the Simultaneous Effect of CuO-H_2O Nanofluid and Receiver Helical Pipe on the Thermal Efficiency of a Cylindrical Solar Collector, *Applied Thermal Engineering, 73* (2014), 1, pp. 1234-1241
[9] Ali Jabari, M., *et al*., Effects of CuO-Water Nanofluid on the Efficiency of a Flat-Plate Solar Collector, *Exp. Therm. Fluid Sci., 58* (2014), Oct., pp. 9-14

[10] Selmi, M., *et al*., Validation of CFD Simulation for Flat Plate Solar Energy Collector, *Renew. Energy, 33* (2008), 3, pp.383-387
[11] Vajjha, R. S., Das, D. K., Experimental Determination of Thermal Conductivity of Three Nanofluids and Development of New Correlations, *International Journal of Heat and Mass Transfer, 52* (2009), 21-22, pp. 4675-4682
[12] Pak, B., Cho, Y. I., Hydrodynamic and Heat Transfer Study of Dispersed Fluids with Submicron Metallic Oxide Particles, *Experimental Heat Transfer, 11* (1998), 2, pp. 151-170
[13] Brinkman, H. C., The Viscosity of Concentrated Suspensions and Solution, *J. Chem. Phys., 20* (1952), 4, pp. 571
[14] Duffie, J. A., Beckman, W. A., *Solar Engineering of Thermal Processes*, 4th ed., John Wiley and Sons, Inc, New York, USA, 2013
[15] Abernethy, R. B., *et al*., ASME Measurement Uncertainty, *ASME. J. Fluids Eng., 107* (1985), 2, pp.161-164
[16] ***, Ansys Fluent 15.0 Users Guide, 2013
[17] Koffi, P. M. E., *et al*, Thermal Performance of a Solar Water Heater with Internal Exchanger using Thermosiphon System in Ivory Coast, *Energy, 64* (2014), Jan., pp. 187-199
[18] Ding, Y., *et al*., Heat Transfer of Aqueous Suspensions of Carbon Nanotubes (CNT nanofluids), *Int. J Heat Mass Transfer, 49* (2006), 1-2, pp. 240-250

Paper submitted: October 5, 2015
Paper revised: December 28, 2015
Paper accepted: January 11, 2016